



# SDSU Water Tunnel Test Section Flow Quality Characterization

José Roberto Moreto<sup>1</sup> and Xiaofeng Liu<sup>2</sup>  
*San Diego State University, San Diego, California, 92182-1308*

**This paper presents a preliminary flow quality characterization of the recently built San Diego State University water tunnel. Conventional planar PIV and time-resolved planar PIV measurements are conducted at selected measurement stations that cover both the freestream and the wall boundary layer regions in the water tunnel test section. Mean velocity, Reynolds normal and shear stresses and turbulence intensity profiles at 25, 50% of test section streamwise locations are presented. Spectra of the turbulent fluctuating velocity at selected wall boundary layer elevations are also be presented. The global r.m.s. variation of the mean velocity in the free stream region is only 1.3% of the mean velocity value.**

## I. Introduction

The characterization of the pressure-related turbulence terms including pressure–rate-of-strain, pressure diffusion and velocity–pressure-gradient tensor in the Reynolds stress transport equation in canonical turbulent flows is of critical importance for calibrating and improving turbulence models for RANS (Reynolds-Averaged Navier Stokes) based flow simulation. Recent work of Liu and Katz (2018)<sup>1</sup> based on planar-PIV clearly shows the complex nature of the pressure related terms and their substantial impact on the dynamics of turbulence transport throughout a shear layer flow past an open cavity. The work also demonstrates the need for a full three-dimensional characterization of the pressure-related terms around the cavity trailing corner. In response to this call, a research project aiming to directly measure all 3D components of the pressure-related terms in Reynolds stress budget for a turbulent shear layer flow past a cavity is currently being carried out at the San Diego State University (SDSU).

To address the call of Liu and Katz (2018)<sup>1</sup> and to extend the investigation of the turbulent shear layer flow past an open cavity, a water tunnel facility was built at San Diego State University (Figure 1). Besides using this facility for the investigation of the cavity flow, it will also be used to introduce advanced lab exercises to engineering students studying fluid mechanics, and to provide a unique research facility to the University to carry out research projects in turbulence, unsteady fluid dynamics, fluid-structure interactions and cavitation.

Before conducting the tomographic PIV measurements of the 3D pressure-related terms in Reynolds stress budget for a turbulent shear layer flow past a cavity, a thorough flow quality characterization of the water tunnel test section is necessary. Detailed flow field characteristics in the test section, including the mean velocity, Reynolds normal and shear stresses and turbulence intensity profiles will be presented in this paper. These data will facilitate future numerical simulations of the tunnel flow and will serve as a preparation for the measurement campaign of the 3D flow characterization of the turbulent cavity shear layer flow.

## II. SDSU Water Tunnel

The San Diego State University (SDSU) water tunnel, as shown in Figure 1, was designed, constructed, assembled and shakedown tested by several groups of SDSU aerospace engineering students starting from fall 2014. This tunnel, similar to the one that the corresponding author used at Johns Hopkins University, is a closed-loop, variable-pressure, and low-turbulence intensity water tunnel suitable for turbulence, cavitation, and unsteady aerodynamics research. The test section of the tunnel has a length of 24” and a cross-section area of 4”×5”, which quadruples the cross-sectional area of the Hopkins tunnel test section of 2”×2.5”. The flow speed of the SDSU water tunnel surpasses 6.4 m/s, giving rise to a Reynolds number of  $1.6 \times 10^5$  per inch at a water temperature of 20°C.

<sup>1</sup> Graduate student, San Diego State University-University of California, San Diego Joint Doctoral Program in Aerospace Engineering, AIAA Student Member.

<sup>2</sup> Assistant Professor, Department of Aerospace Engineering, SDSU. AIAA Associate Fellow. Email: Xiaofeng.Liu@sdsu.edu.



Figure 1: San Diego State University water tunnel test section.

### III. Water tunnel flow quality characterization

The first step towards the accurate measurement of all the Reynolds stress components is the base flow characterization. In order to discern between the test geometry effect on the flow and the possible fluctuations already in the water tunnel flow, it is necessary to perform a flow survey of the test section without the test model installed. The flow survey is conducted in two phases: a preliminary flow assessment to identify opportunities for improvements on the flow quality, and a final flow characterization to define the free flow condition. The complete flow characterization has been carried out at two streamwise measurement stations, which are located at 6 and 12 inches (corresponding to 25% and 50% test section length) downstream of the inlet of the test section, respectively, as shown in Figure 2. At each streamwise measurement station, flow survey is conducted using Particle Image Velocimetry (PIV) within three parallel vertical planes separated in spanwise direction at 1.0 inch apart, with the central plane located at the central span location. As shown in Figure 2, each measurement plane consists of 5 stacked Field of Views (FOV), with each FOV of 1.0×1.0 inch square in size.

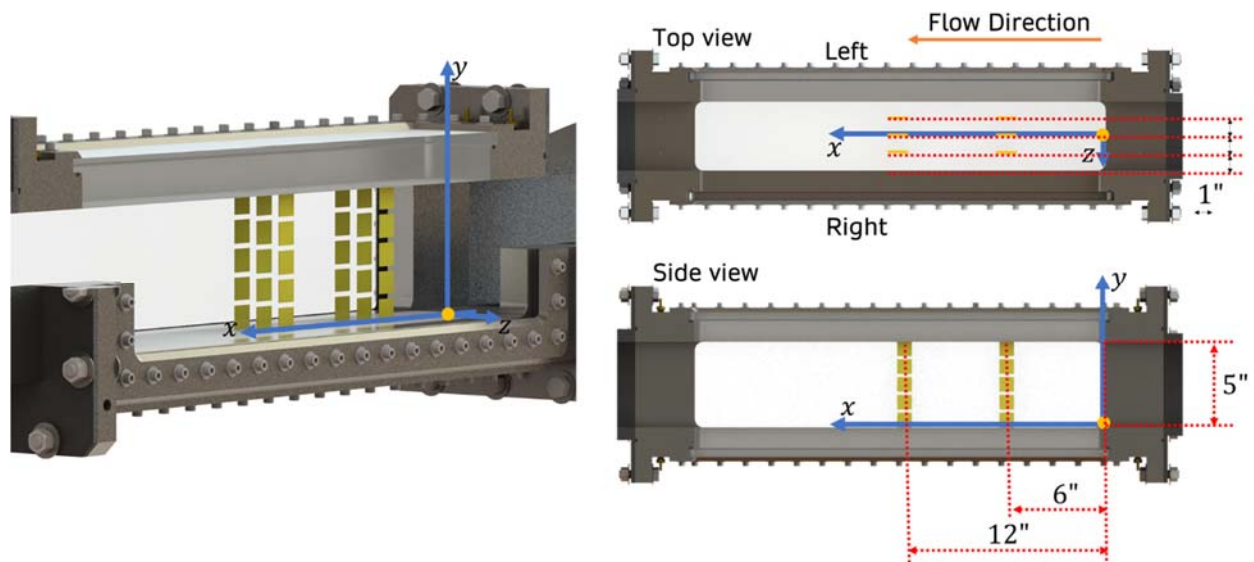
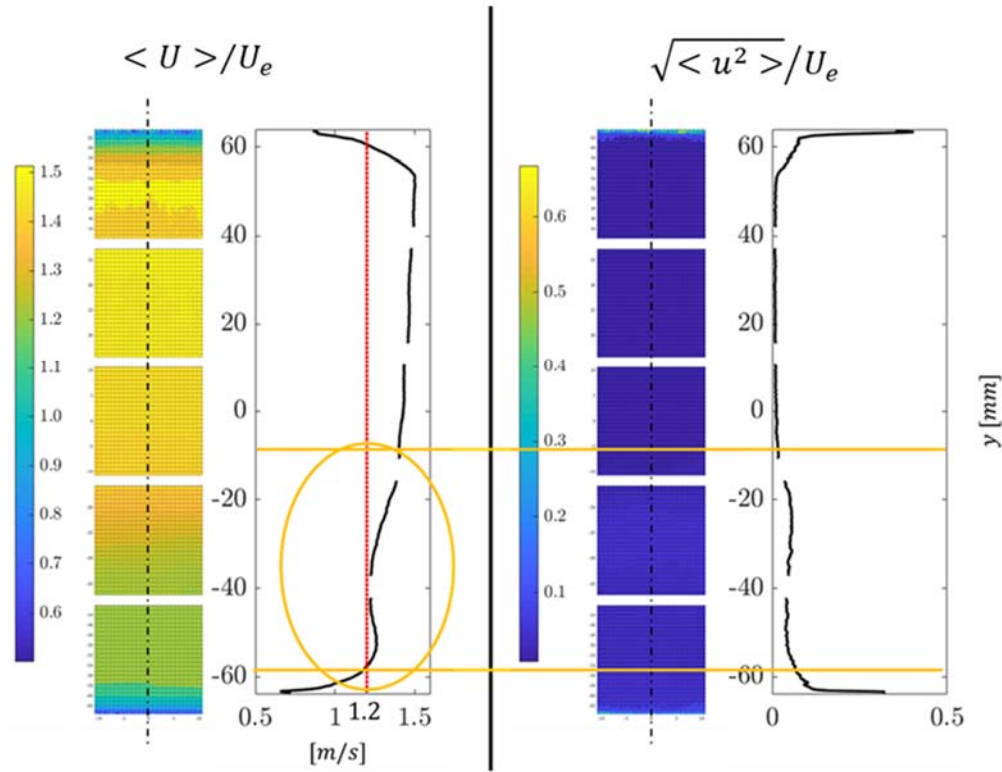


Figure 2: Location of measurement stations for flow characterization survey in the water tunnel test section. The golden squares show the field of view (FOV) used to acquire the PIV images, with each FOV of 1.0×1.0 inch square in size.



**Figure 3: Average velocity and r.m.s. velocity profiles 12” downstream of the test section inlet obtained from the initial flow survey for the water tunnel test section at the central span plane, with velocity defect due to damaged honeycomb highlighted. This defect was corrected by replacing the damaged honeycomb with a brand new one (see Figure 4).**

The preliminary velocity measurement was conducted using a double exposure PIV. The double exposure frames are acquired at a frequency of 5.0 Hz and the time separation between frames was 233 $\mu$ s. The measurements for this initial evaluation are carried out at central measurement plane only. The free stream speed is set to 1.2m/s in order to facilitate comparisons with the two-dimensional open cavity shear layer flow investigations of Liu and Katz (2013<sup>2</sup> and 2018<sup>1</sup>), which has a Reynolds number of  $4.0 \times 10^4$  based on the cavity length of 1.5 inch.

The initial flow survey indicated there was an momentum defect close to the lower region of the test section, as shown in **Figure 3** with a highlighted circle. This momentum defect is due to a small damage occurring on the honeycomb upstream of the test section. After replacing the damaged honeycomb, the flow was surveyed again at the same location. The new survey result indicates an improved velocity profile without momentum loss, as shown in Figure 4. Once the problem was resolved, we performed a complete survey at all the regions shown on **Figure 2**. The procedure for the flow characterization follows that proposed by Spedding *et al.*<sup>3</sup> (2009). For each plane defined in Figure 2, the velocity profile, boundary layer displacement thickness, momentum thickness, Reynolds stresses and the turbulence intensity are obtained. Some authors<sup>4,5</sup> report the turbulence intensity as the streamwise r.m.s. velocity fluctuation. In this work we adopt the turbulence intensity defined in Spedding *et al.*<sup>3</sup> (2009) as shown below.

$$u' = \sqrt{\langle u^2 \rangle + \langle v^2 \rangle + \langle w^2 \rangle} \quad (1)$$

where  $u$  is the streamwise velocity fluctuation,  $v$  and  $w$  are fluctuations normal to the mean flow and are assumed to have the same magnitude<sup>3</sup> i.e.,  $v \approx w$ . The symbol  $\langle \rangle$  denotes temporal averaging of the quantity, and the velocity component fluctuations are defined as:

$$\begin{aligned} u &= U - \langle U \rangle \\ v &= V - \langle V \rangle \\ w &\approx v \end{aligned} \quad (2)$$

Reynolds stress and velocity components are non-dimensionalized by  $U_e$ , which is the average streamwise velocity measured far from the walls, i.e., above the edge of the wall boundary layer.

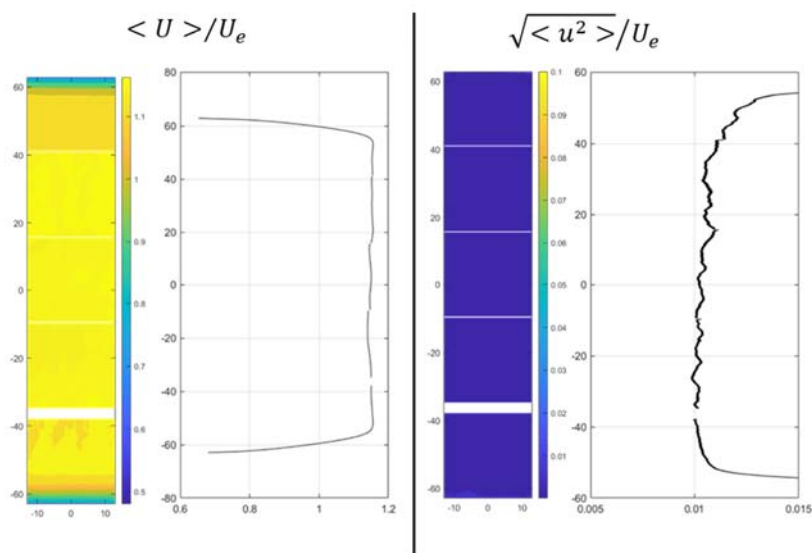


**Figure 4: Average velocity and fluctuation profiles 12” downstream of the test section inlet based on 3149 velocity vector maps after replacing the honeycomb. Note that no fine screen is installed upstream of the test section for this measurement.**

## IV. Measurement Results

### Initial flow assessment

After the damaged honeycomb was replaced, the velocity profile at the center plane 12” downstream of the inlet of the test section was obtained by a 2D PIV measurement. A total of 3149 image pairs were obtained at each of the 5 elevation positions at the central plane (reference **Figure 2**). The 2D velocity flow field is obtained using the Davis 7 software. As shown in Figure 4, the velocity fluctuation ( $\sqrt{\langle u^2 \rangle} / U_e$ ) is about 1.0% in the free stream region in the test section. Please note that, although we do have fine screen made of stainless steel available, for the current measurement, the fine screen is not installed upstream of the test section. The free stream turbulence intensity is presumably to be smaller than 1.0% if the fine screen is installed (to be verified in the next stage of this investigation).

### Detailed Flow assessment

The flow assessment is performed at all the locations as indicated in **Figure 2** by following the coordinate system described in the same figure. There are a total of 30 measurement field of view (FOV) locations involved in the flow survey and the coordinates of the center of the lower edge of the FOV are shown in **Table I**. The location coordinates are shown in inches and are nondimensionalized by the water tunnel height  $L$  ( $L = 5$ ”). Also the last column presents the reference velocity  $U_e$  used for flow nondimensionalization.

All the measurements are performed at the same flow conditions. The experimental setup for the time-resolved, two-dimensional PIV measurements is similar to the one used by Liu and Katz<sup>2</sup> (2013). We used a Photonics DM40-527 Nd:YLF laser that has a maximum pulse rate of 10 kHz. The images are recorded at 4500 frames per second using a PCO.dimax CMOS camera, at a resolution of  $1008 \times 1000$  pixels, giving a Nyquist frequency of 2250 Hz for the measured velocity vectors. To synchronize the laser with the camera, we use Quantum Composer model 9518 pulse generator. The size of the field of view (FOV) is  $25 \text{ mm} \times 25 \text{ mm}$ . With an appropriate concentration of seed particles, 8–12  $\mu\text{m}$  diameter hollow glass spheres with specific gravity of 1.05–1.15, we are able to use an interrogation window size of  $32 \times 32$  pixels, corresponding to physical size of  $0.8 \text{ mm} \times 0.8 \text{ mm}$ . With a 75% window overlap, a measurement grid size of  $0.4 \text{ mm} \times 0.4 \text{ mm}$  is achieved.

**Table 1: Measurement Field of View locations.**

Measurement sequential number	FOV x [in]	y [in]	z [in]	x/L	y/L	z/L	Ue [m/s]
01	12	0	0	2.4	0.0	0.0	1.165
02	12	1	0	2.4	0.2	0.0	1.162
03	12	2	0	2.4	0.4	0.0	1.178
04	12	3	0	2.4	0.6	0.0	1.179
05	12	4	0	2.4	0.8	0.0	1.194
06	12	0	1	2.4	0.0	0.2	1.184
07	12	1	1	2.4	0.2	0.2	1.158
08	12	2	1	2.4	0.4	0.2	1.180
09	12	3	1	2.4	0.6	0.2	1.194
10	12	4	1	2.4	0.8	0.2	1.209
11	12	0	-1	2.4	0.0	-0.2	1.168
12	12	1	-1	2.4	0.2	-0.2	1.167
13	12	2	-1	2.4	0.4	-0.2	1.163
14	12	3	-1	2.4	0.6	-0.2	1.173
15	12	4	-1	2.4	0.8	-0.2	1.188
16	6	0	0	1.2	0.0	0.0	-
17	6	1	0	1.2	0.2	0.0	1.158
18	6	2	0	1.2	0.4	0.0	1.145
19	6	3	0	1.2	0.6	0.0	1.157
20	6	4	0	1.2	0.8	0.0	1.184
21	6	0	1	1.2	0.0	0.2	1.151
22	6	1	1	1.2	0.2	0.2	1.151
23	6	2	1	1.2	0.4	0.2	1.159
24	6	3	1	1.2	0.6	0.2	1.156
25	6	4	1	1.2	0.8	0.2	1.199
26	6	0	-1	1.2	0.0	-0.2	1.146
27	6	1	-1	1.2	0.2	-0.2	1.165
28	6	2	-1	1.2	0.4	-0.2	1.157
29	6	3	-1	1.2	0.6	-0.2	-
30	6	4	-1	1.2	0.8	-0.2	1.165

For each measurement FOV locations listed in **Table 1**, a total of 25393 consecutive PIV images, which corresponds to 5.64 seconds of acquisition duration time, are acquired during the detailed flow survey. However, due to the large amount of time required for processing the entire sets of data, as a preliminary analysis, the velocity fields presented here are only based on the first 2501 frames (~10% data from the entire PIV image datasets) acquired at each location, which correspond to 0.556 seconds of recording time. The velocity vectors are computed by the Dynamic Studio Edu PIV 6.8 software using the adaptive PIV method with a maximum interrogation window size of  $64 \times 64$  pixel<sup>2</sup> and a minimum interrogation window size of  $32 \times 32$  pixel<sup>2</sup>, at a grid step of  $8 \times 8$  pixel<sup>2</sup>. After the preliminary calculation, the velocity vector fields are dewarped using an image of a calibration target that has a dotted pattern with 0.5mm diameter dots spaced 1mm apart in the x and y-directions. After the post-processing of the velocity vectors, a total of 28 datasets listed in Table 1, except those in Measurement No. 26 and 29, are considered valid. The results for all the valid dataset are presented below.

To show the overall picture of the flow survey results, **Figure 5** presents the mean velocity and the turbulence intensity profiles at the valid measurement locations. The velocity and velocity fluctuations profiles are averaged along the x-direction within the FOV at the measurement plane, assuming the streamwise pressure gradient is negligible with the 1-inch FOV of measurements.

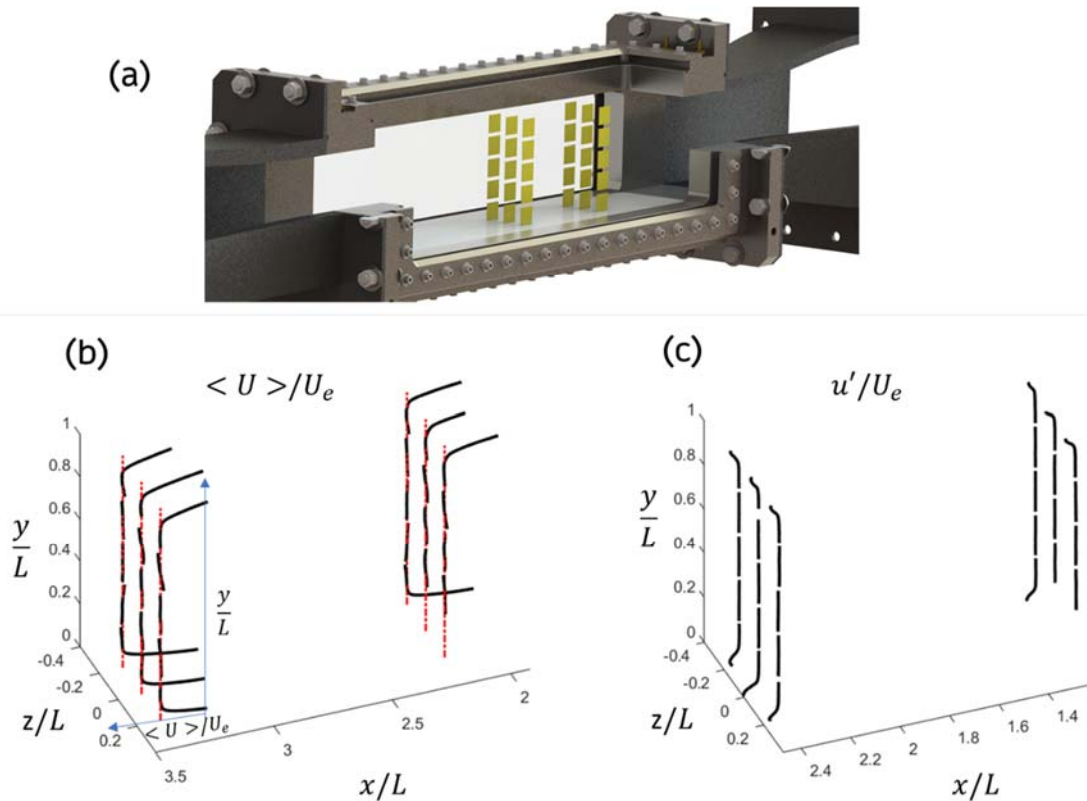


Figure 5: Average velocity and turbulence intensity profiles at the measurement FOV locations. (a) Measurement FOV location. (b) Average velocity profile. (c) turbulence intensity profile.

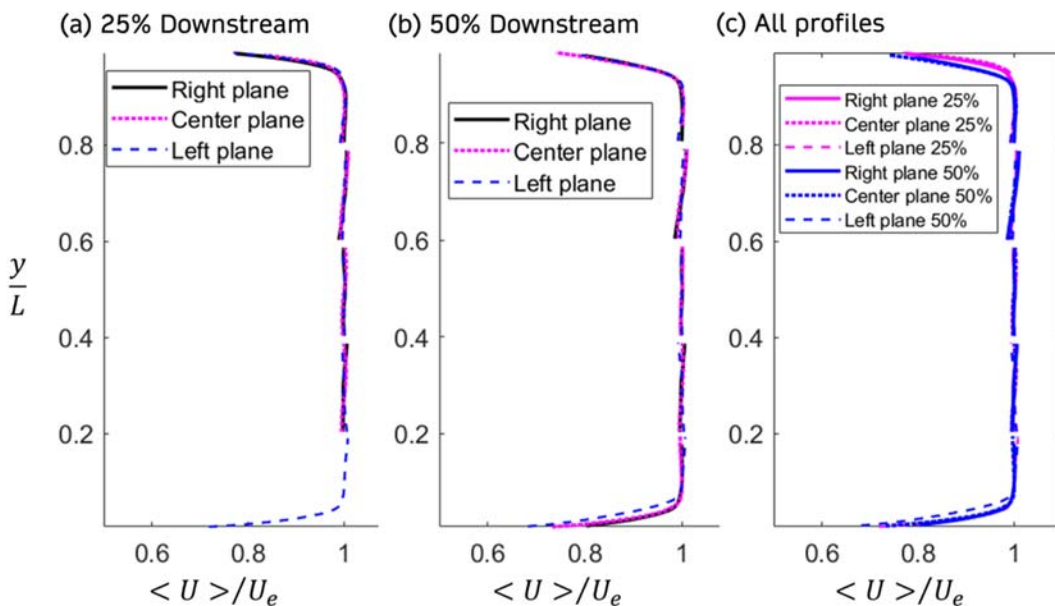
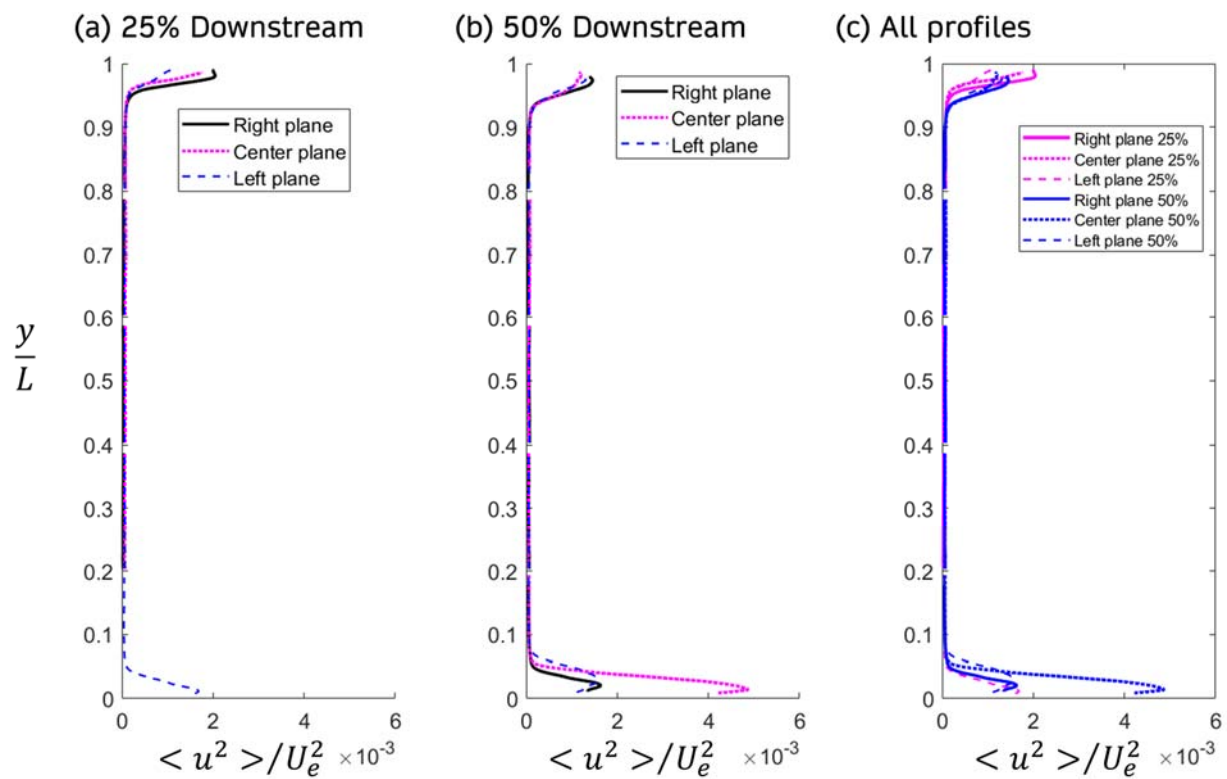


Figure 6: Averaged  $u$ -component velocity profiles. (a) profiles at 25% downstream of the test section inlet. (b) profiles at 50% downstream of the test section inlet. (c) comparison of all valid velocity profiles. See Figure 2 for coordinate system and references.

To have a close examination of these mean velocity profiles, Figure 6 presents the averaged  $u$ -component velocity profiles at 25% and 50% (of test section length) streamwise locations downstream of the test section inlet, respectively, as well as the comparison of all valid velocity profiles at those locations. The velocity profile shown on **Figure 6** has

a uniform flow region from  $y/L = 0.1$  up to  $y/L = 0.9$ . As shown in Figure 6(c), at the region close to the top window the boundary layer thickness at the 50% streamwise location is thicker than that at the 25% streamwise location. The slanted profile in the region between  $y/L = 0.6$  and 0.8 is presumably due to misalignment of the measurement FOV at that location.

The Reynolds normal and shear stress profiles are presented in Figures 7, 8 and 9, respectively. As can be seen in **Figure 7**, the  $\langle u^2 \rangle$  component of the Reynolds stress tensor are in agreement with the expected shape for a channel flow (Pope, 2000)<sup>6</sup>. Similar agreement with (Pope, 2000)<sup>6</sup> is observed for Figures 8 and 9. However, close to the walls some profiles such as  $\langle v^2 \rangle$  and  $-\langle uv \rangle$  at the center planes are either not smooth, or the magnitude appears to be overestimated in comparison with  $\langle u^2 \rangle$ . This is an indication that these second-order turbulence statistics may not be converged at those wall boundary layer regions based on only  $\sim 10\%$  of the data from the entire PIV image datasets. To ensure convergence of the second-order turbulence statistics at the boundary layer regions, more processed velocity data from perhaps the entire PIV image datasets are needed. Apparently the convergence requirements for these second order turbulence statistics within the range of  $0.15 < y/L < 0.85$  are greatly alleviated because of the low turbulence intensity in the free stream region.



**Figure 7:** Reynolds normal stress  $\langle u^2 \rangle$  profiles. (a) profiles at 25% downstream of the test section inlet. (b) profiles at 50% downstream of the test section inlet. (c) comparison of all valid profiles.

**Table 2. Turbulence statistics in the free stream region.**

	$u'/U_e$	$\langle u^2 \rangle / U_e^2$	$\langle v^2 \rangle / U_e^2$	$-\langle uv \rangle / U_e^2$	$\sqrt{\langle u^2 \rangle} / U_e$	$\sqrt{\langle v^2 \rangle} / U_e$	$\sqrt{ \langle uv \rangle } / U_e$
Average	0.0128	5.78E-05	5.50E-05	-1.82E-06	7.50E-03	7.30E-03	1.40E-03
std	0.0019	1.27E-05	1.58E-05	2.04E-06	9.11E-04	1.30E-03	5.72E-04

Table 2 summarizes the turbulence statistics in the freestream region. From the table, it can be seen that the turbulence intensity in terms of  $u'$  defined in equation (1) is about 1.3%. Please note that if the stainless steel screen is installed, the turbulence intensity level is presumably smaller. Comparison of the turbulence intensity profiles across the tunnel test section is shown in Figure 10. The disparities shown in Figure 10 is possibly due to lack of convergence for the high order turbulence based on only 10% of entire PIV datasets. This issue will be solved by enlarging the ensemble size involved in the turbulence statistics calculation.

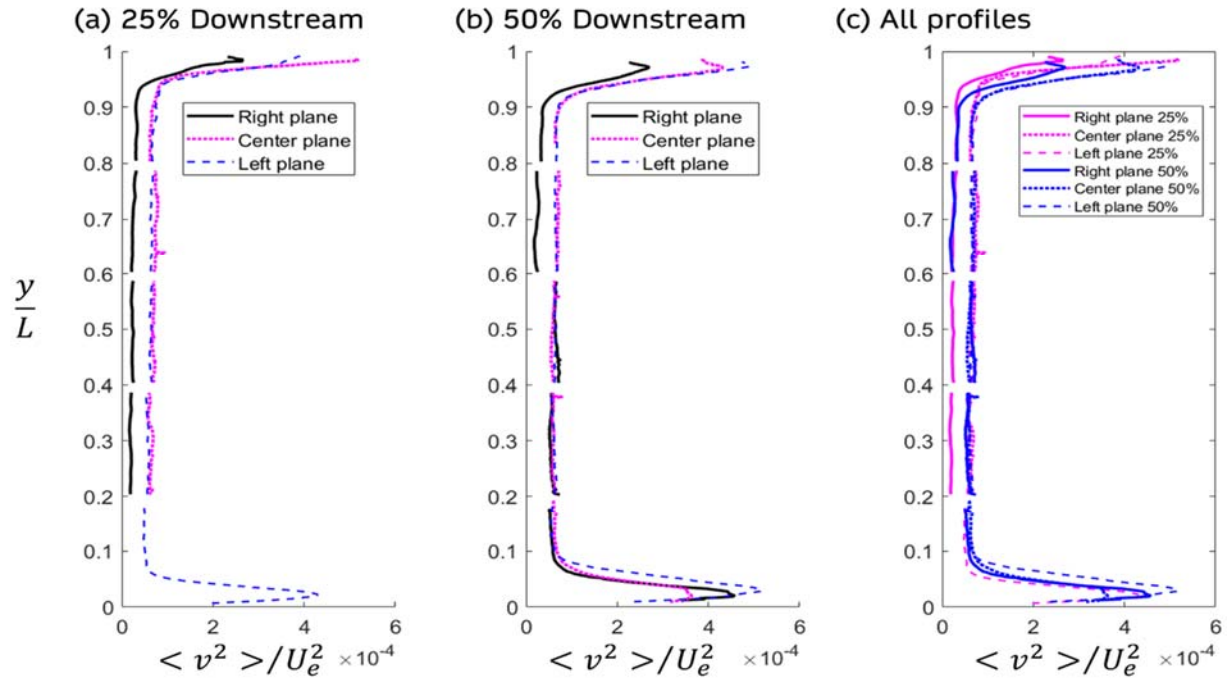


Figure 8: Reynolds normal stress  $\langle v^2 \rangle$  normalized by the reference pressure profiles. (a) profiles 25% downstream of the test section inlet. (b) profiles 50% downstream of the test section inlet. (c) All valid profiles. See Figure 2 for coordinate system.

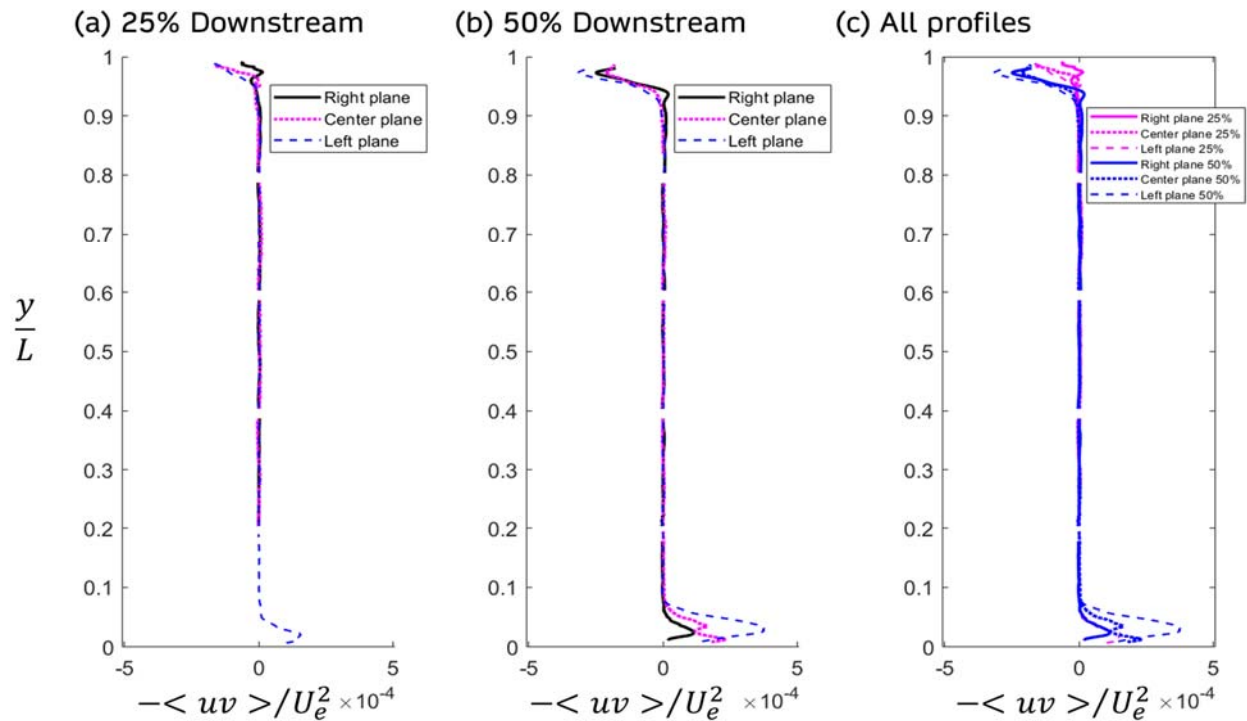


Figure 9: Reynolds shear stress  $-\langle uv \rangle$  profiles. (a) profiles at 25% downstream of the test section inlet. (b) profiles at 50% downstream of the test section inlet. (c) comparison of all valid profiles. See Figure 2 for coordinate system definition.

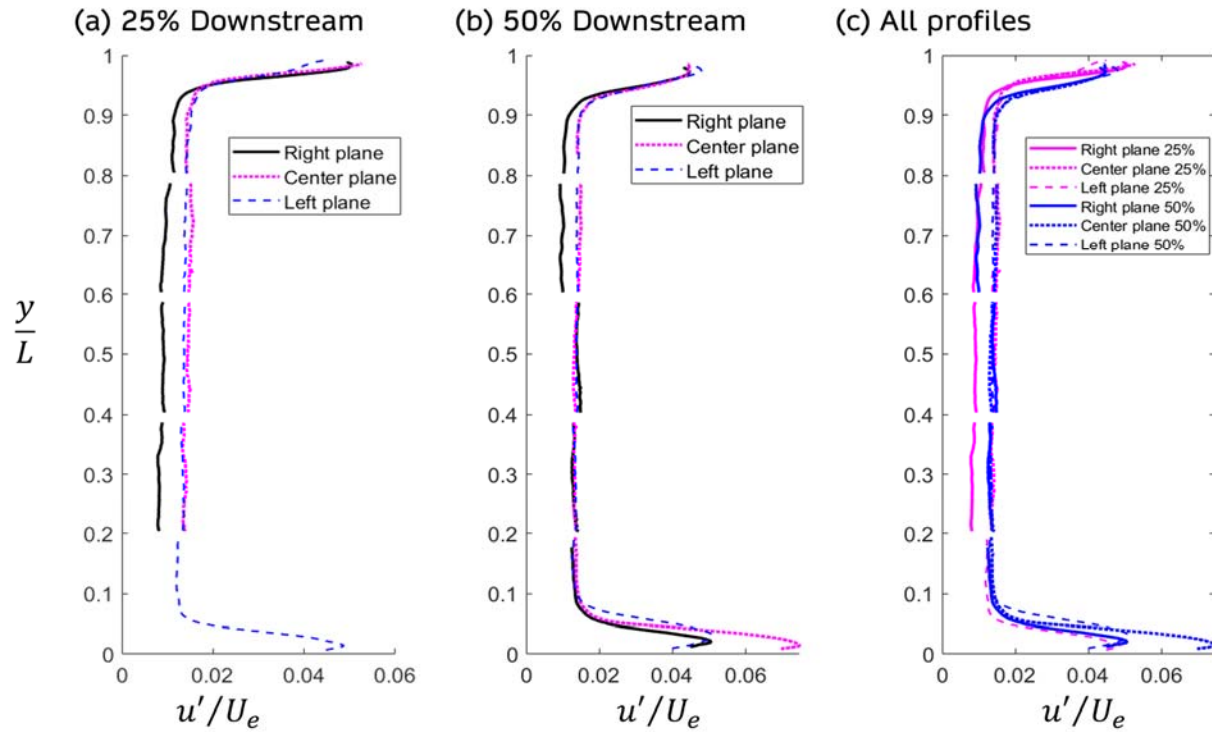


Figure 10: Turbulence intensity profiles. (a) profiles at 25% downstream of the test section inlet. (b) profiles at 50% downstream of the test section inlet. (c) comparison of all valid profiles.

In addition to the mean turbulence statistics profiles across the tunnel test section,  $u$ -component fluctuation velocity power spectra at representative locations within the wall boundary layer is also presented in **Error! Reference source not found.** so as to facilitate the understanding of the frequency composition of the flow field. As shown in Figure 10, the velocity spectra are in agreement with Kolmogorov's  $-5/3$  law. Also there is no significant peaks observed in those spectra, indicating that for the empty tunnel test section, there is no significant periodic motion in the wall turbulence flow field.

## V. Conclusion

The SDSU water tunnel flow assessment is in progress. The initial flow evaluation provides valuable information to improve the flow quality and for the necessary equipment and facility adjustment. Additionally, we performed flow assessments under the condition without installing a turbulence suppressing screen. The data analysis shows a uniform flow occurs within the range of 10% to 90% of the tunnel height. The turbulence intensity in the freestream region is 1.3%, with a standard deviation of 0.2% based on the preliminary data analysis.

The uniformity of the freestream region in terms of both turbulence statistics and mean flow spatial variation is

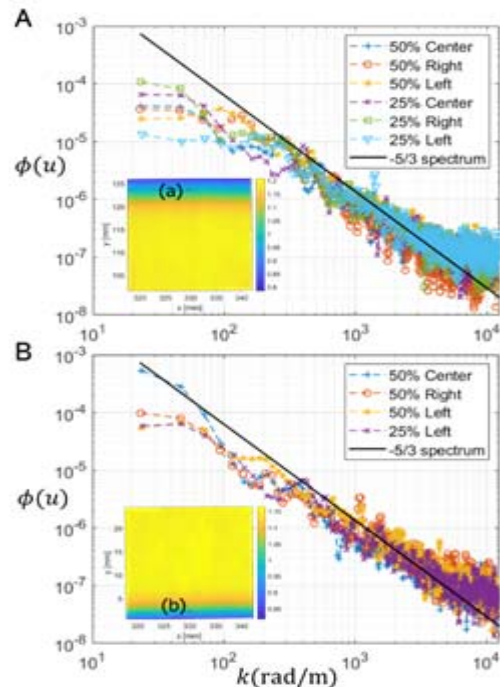


Figure 11: Velocity power spectral density (PSD) at selected locations. A is the PSD obtained at the top wall boundary layer at the location (a) depicted in the inset. B is the PSD obtained at the bottom wall boundary layer at the location (b) depicted in the inset.

acceptable based on the preliminary data analysis. The global r.m.s. variation of the mean velocity is only 1.3% of the mean velocity value.

Due to the large amount of data generated by time-resolved PIV measurements, it is not viable to survey the entire space in the test section. However, the results obtained provide guidance for selection of representative flow regions for the characterization of the water tunnel flow quality.

An evaluation of a screen for turbulence suppression will be performed and compared with the flow characterization without the screens. This will enable us to determine the final configuration of the water tunnel for the 3D velocity and pressure field measurements for the turbulent cavity shear layer flow investigation.

### Acknowledgments

This work has been sponsored in part by the San Diego State University UGP program 2015 and in part by the Office of Naval Research grant N00014-19-1-2020 (K.-H. Kim is the Program Officer). J.R. Moreto acknowledges the support of the 2018/19 University Graduate Fellowship from the San Diego State University.

### References

- 1 Liu, X., and Katz, J., "Pressure–Rate-of-Strain, Pressure Diffusion, and Velocity–Pressure-Gradient Tensor Measurements in a Cavity Flow," *AIAA Journal*, vol. 56, Oct. 2018, pp. 3897–3914.
- 2 Liu, X., and Katz, J., "Vortex-corner interactions in a cavity shear layer elucidated by time-resolved measurements of the pressure field," *Journal of Fluid Mechanics*, vol. 728, Aug. 2013, pp. 417–457.
- 3 Spedding, G. R., Hedenström, A., and Johansson, L. C., "A note on wind-tunnel turbulence measurements with DPIV," *Experiments in Fluids*, vol. 46, 2009, pp. 527–537.
- 4 Örlü, R., Fiorini, T., Segalini, A., Bellani, G., Talamelli, A., and Alfredsson, P. H., "Reynolds stress scaling in pipe flow turbulence - First results from CICLoPE," *Philosophical Transactions of the Royal Society A: Mathematical, Physical and Engineering Sciences*, vol. 375, Mar. 2017.
- 5 Scharnowski, S., Bross, M., and Kähler, C. J., "Accurate turbulence level estimations using PIV/PTV," *Experiments in Fluids*, vol. 60, Jan. 2019.
- 6 Pope, S. B., *Turbulent Flows*, Cambridge: Cambridge University Press, 2000.